In Silico Electrophysiological Evaluation of Scaffold Geometries for Cardiac Tissue Engineering

Ricardo M Rosales[1,2], Konstantinos A Mountris[1,2], Manuel Doblaré[1,2], Manuel M Mazo[3,4], Esther Pueyo[1,2]

[1] Aragon Institute of Engineering Research, University of Zaragoza, IIS Aragon, Zaragoza, Spain
[2] CIBER in Bioengineering, Biomaterials & Nanomedicine (CIBER-BBN), Spain
[3] Regenerative Medicine Program, CIMA Universidad de Navarra, Pamplona, Spain
[4] Hematology and Cell Therapy, Clínica Universidad de Navarra, Pamplona, Spain

Abstract

Human induced pluripotent stem cell-derived cardiomyocytes (hiPSC-CMs) cultured on bio-printed scaffolds have shown promising results for cardiac function restoration in regenerative medicine. Nevertheless, pro-arrhythmicity favored by reduced conduction velocity of the transplanted constructs as compared to native tissue has been poorly assessed. Here, we investigate the impact of the scaffold geometry on the electrical activation properties of hiPSC-CMs cultures.

Electrophysiological models of hiPSC-CMs and the Finite Element Method were employed for computational simulation of hiPSC-CMs cultures. The models were calibrated to replicate experimentally measured activation time maps by adjusting parameters representative of fiber alignment and cell-to-cell coupling. Scaffolds with rectangular, auxetic and elongated hexagonal pore shapes were studied to determine the most biomimetic structure in terms of electrical propagation characteristics.

Our results showed that the geometry with elongated hexagonal pores led to faster activation of hiPSC-CMs cultures by facilitating the alignment of cardiac fibers in the longitudinal direction. These pore shapes mimic cardiac anisotropy, therefore would be the preferred geometry for experimental culture.

1. Introduction

Tissue engineering has emerged as a promising solution to restore cardiac function through transplantation of human induced pluripotent stem cell-derived cardiomyocytes (hiPSC-CMs) into ventricular regions damaged due to e.g. myocardial infarction [1]. Several studies have been conducted to evaluate in vitro maturation of hiPSC-CMs and how this can be improved by culturing cells with the aid of three-dimensional (3D) scaffolds [2–4]. This latter approach has been reported to improve cell-to-cell connectivity, by rising the number of gap junctions per cell, and replication of the cardiac anisotropy, by orienting the cells in a preferential direction.

Electrical propagation in tissue engineered patches should be temporarily synchronized with that of the surrounding healthy tissue in order to reduce the probability of developing arrhythmic events. Considering that slow conducting regions in a tissue favor reentrant arrhythmias [5], it is advisable that the activation time (AT) in the engineered construct is as similar as possible to the one of the native tissue that has been lost as a consequence of e.g. myocardial infarction. Further extensive studies are needed to define optimal scaffold structures that produce physiological propagation and AT values as in healthy ventricular tissues [6].

Computational power and memory capacity have increased drastically in the past decades, which has been accompanied by remarkable improvements in experimental data collection and processing. These scientific and technological breakthroughs make it possible to simulate biological processes in a faster and more accurate manner. In particular, cardiac electrical modeling and simulation have already shown capacity to aid in the identification of sources that make hiPSC-CMs more prone to develop arrhythmic behaviors in response to drugs or in the presence of disease [7, 8].

The aim of this work is to gain insight into the electrical activation of hiPSC-CMs cultured in 3D scaffolds and assess the effect of the scaffold geometry. In silico models with square pore scaffolds were created and Finite Element Method (FEM) simulations were run to compute AT maps. The models were calibrated to match in vitro AT maps calculated from optical mapping experiments. Additionally, in silico scaffolds with rectangular, auxetic and elongated hexagonal (honeycomb) pore shapes were built and the one leading to shorter global ATs was identified.

2. Materials and Methods

2.1. Electrophysiological modeling

The electrophysiology of hiPSC-CMs was described by the ventricular-like action potential model of Paci et al. [9], which follows the Hodgkin & Huxley formulation. Electrical propagation in coupled cells was described by the monodomain model according to the following reaction-diffusion partial differential equation:

$$\begin{aligned} \partial V/\partial t &= \boldsymbol{\nabla} \cdot (\boldsymbol{D}\boldsymbol{\nabla} V) - I_{ion}(V)/C \quad && \text{in } \Omega \\ \boldsymbol{n} \cdot (\boldsymbol{D}\boldsymbol{\nabla} V) &= 0 && \text{in } \partial\Omega \end{aligned} \tag{1}$$

where V is the transmembrane voltage and I_{ion} the total current, including all ionic currents and the stimulus current. C is the membrane capacitance, $\boldsymbol{D}$ the diffusion tensor, Ω the cardiac domain and $\partial\Omega$ the boundary of Ω.

Mesh representations of cultured hiPSC-CMs (tissue) and scaffolds were constructed using quadrilateral and hexahedral elements for two-dimensional (2D) and 3D cases, respectively. Tissue node spacing was set at $31\,\mu\mathrm{m}$ as it is the pixel resolution in optical data, as well as, is consistent with the time and accuracy trade-off of computations. Scaffold node spacing was adjusted to ensure proper tissue nodes alignment, while orienting them following the direction of the scaffold walls.

Mesh and model information were input to the in-house software *ELECTRA* [10, 11], which uses a dual adaptive explicit method [12] for solving the reaction and diffusion terms in (1). This method enhances computational efficiency while maintaining numerical precision. A transverse-to-longitudinal conductivity ratio of 0.15 was set, in agreement with the reported anisotropy in conduction velocity of the cardiac tissue [13]. After initializing the models to steady-state, each simulation consisted of three $1\,\mathrm{Hz}$-paced cycles, with the last cycle being used for AT calculation. Stimuli of $5\,\mathrm{nA}$-magnitude and $2\,\mathrm{ms}$-duration were applied.

2.2. Model calibration

In silico models with square pore scaffolds were calibrated based on in vitro optical mapping data. For these experiments, melt electrowriting (MEW) was used to fabricate $5 \times 5 \times 0.45\ \mathrm{mm}^3$ constructs with square pores of $200\,\mu\mathrm{m}$-side, on which hiPSC-CMs were placed. 3D MEW-based cultures were optically mapped to obtain high-resolution calcium transient measurements along time. These video data was analyzed using the in-house software *OMap*, which applies temporal and spatial filtering and calculates AT values for every pixel [14].

Once a clean image of an AT map was obtained by performing opening, closing and median filtering (Figure 1a), a dendrogram was used to cluster the per-pixel AT values according to the Euclidean distance of the clusters centroids. Node sets in the in silico tissue models were defined based on this classification, as depicted in Figure 1b. The stimulus current was applied onto the node set initiating the depolarization (i.e. with the shortest AT), which is shown in red in the figure.

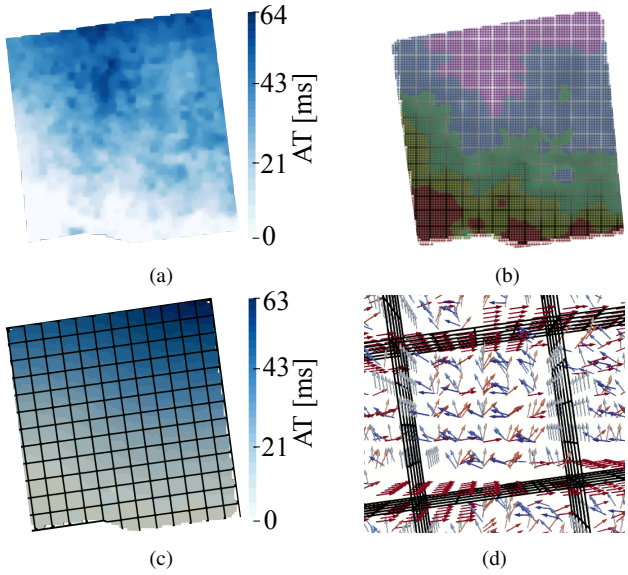

Figure 1: (a) Experimental AT map obtained from optical mapping. (b) In silico mesh generation and definition of node sets. (c) Simulated AT map. (d) Tissue node alignment.

The tissue mesh was embedded in the scaffold mesh. Tissue nodes within a distance of $27\,\mu\mathrm{m}$ to the scaffold were aligned with the direction of the pore walls, as depicted in Figure 1d. The distance threshold was chosen in agreement with experimentally reported values [4]. As a final step, the longitudinal conductivity was adjusted so that the maximum AT values in the simulated map (Figure 1c) matched the experimental ones.

2.3. Variations in scaffold geometry

Electrical wave propagation was simulated in both 2D and 3D in silico patches composed of the scaffold and the tissue. A tissue mesh of $2 \times 4\ \mathrm{mm}^2$ was generated for 2D cases and a mesh with the same size and thickness of $0.45\,\mathrm{mm}$ was used for 3D cases. Before introducing the scaffold, all tissues were set to have the same random fiber orientation following a uniform statistical distribution spanning 0-180 degrees in plane. In 3D cases, the cellular orientation was additionally set to be consistent with a normal distribution with zero mean along the construct's thickness. After including the scaffold, tissue nodes within $65\,\mu\mathrm{m}$ from the pores walls were oriented according to the

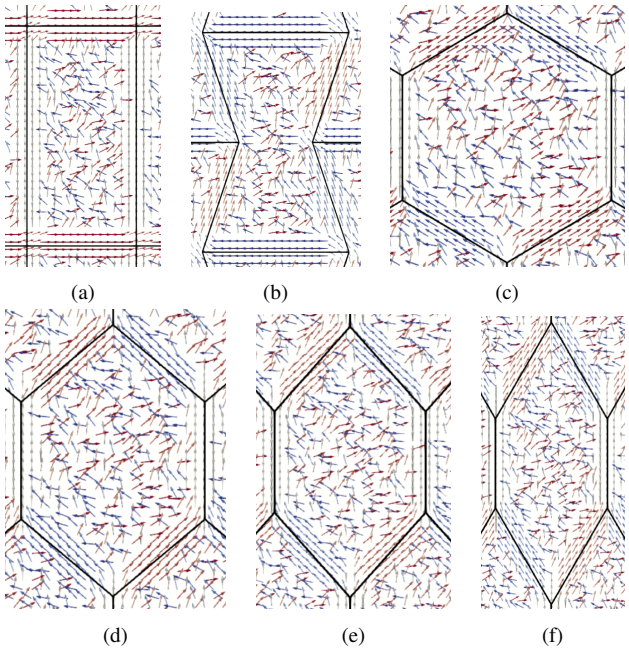

Figure 2: Pore geometries and fiber alignments: (a) rectangular; (b) auxetic; (c), (d), (e) and (f) hexagonal elongated by 120, 100, 80 and 60 degrees.

wall direction (Figure 2). This higher distance threshold, in comparison with the one aforementioned in 2.2, was used to emphasize the effect of scaffold's geometry. Based on model calibration and in values reported in [12], a diffusion coefficient of $4.22 \times 10^{-4}\,\mathrm{cm/ms^2}$ was associated with 100% alignment of tissue nodes. A linear relationship was defined between alignment percentages and diffusion coefficient values.

We analyzed scaffolds with the following pore shapes: rectangle; elongated hexagons with angles of 120, 100, 80 and 60 degrees; and perpendicular and parallel to the depolarizing direction auxetic architectures. All configurations were generated by maintaining a constant pore area of $0.4\,\mathrm{mm^2}$ (Figure 2). The rectangular, parallel auxetic and 60-degree elongated hexagonal cases were further evaluated with a more clinically relevant size of $5 \times 20 \times 0.45$ $\mathrm{mm^3}$.

3. Results

As can be seen by comparing Figures 1a and 1c, a close match between simulated and real AT maps was obtained by adjusting the value of the diffusion coefficient in the monodomain model. A difference of $1\,\mathrm{ms}$ between the maximum AT values was found for the optimal longitudinal diffusion coefficient, set to $3.5 \times 10^{-5}\,\mathrm{cm/ms^2}$.

The seven tested scaffold architectures yielded similar trends in maximum AT values between 2D and 3D numerical simulations, as shown in Figure 3. Alignment percentages were higher for rectangular and auxetic than for hexagonal configurations. Among hexagonal ones, alignment increased from 120-degree to 60-degree elongated pores. Nevertheless, the maximum AT was found to be shorter for 60-degree elongated hexagons than for other pore geometries.

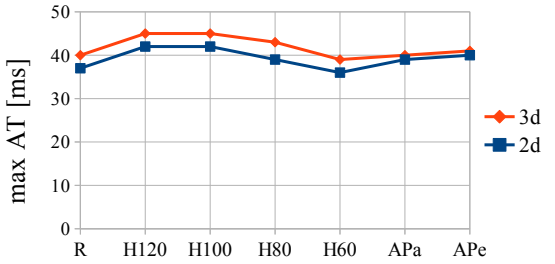

Figure 3: Maximum AT values for 2D and 3D tissue-scaffold architectures. R: rectangular, APa: Parallel oriented auxetic, APe: Perpendicularly oriented auxetic and HX: Hexagonal elongated by X degrees.

As expected, larger values of maximum AT were found when increasing the size of the tissue and the scaffold. Results for $5 \times 20 \times 0.45\ \mathrm{mm^3}$ constructs are shown in Figure 4. Similarly to the small constructs, the most elongated hexagonal geometry was found to conduct faster than the other geometries, with differences between geometries of up to $36\,\mathrm{ms}$.

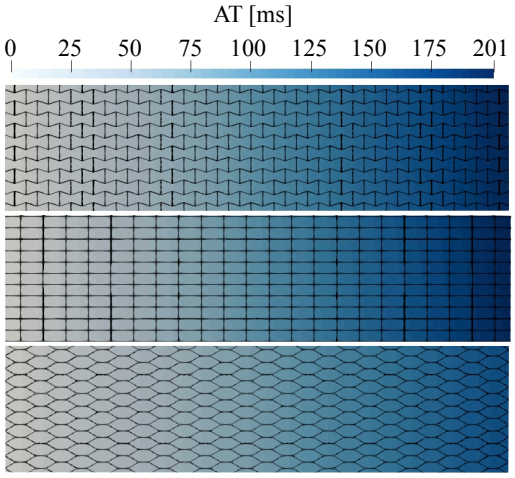

Figure 4: From top to bottom: AT for $5 \times 20 \times 0.45\ \mathrm{mm^3}$ rectangular, parallel oriented auxetic and 60-degree elongated hexagonal scaffolds.

4. Discussion

In silico electrophysiological modeling and simulation was used to characterize electrical activation of hiPSC-

CMs cultured on scaffolds of different geometries and to identify the one leading to more physiological ATs. We replicated experimentally measured AT maps through simulations for the case of scaffolds with square pores. When assessing the effect of other pore shapes computationally, we showed that, even though elongated hexagons were associated with lower cellular alignment than rectangular or auxetic structures, they led to faster conduction. This was due to the fact that most elongated hexagons better mimic cardiac anisotropy by orienting more fibers parallel to the direction of the depolarization wavefront. The advantage of this geometry was even more emphasized when larger tissue-scaffold sizes were tested, which would point to this geometry as the most suited one to minimize arrhythmic risk after transplanting a construct into a damaged heart. These results set the basis for further investigations into tissue engineered assisting devices that ensure cardiac functionality restoration avoiding significant alterations in the electrical activity that could be pro-arrhythmic.

Acknowledgments

This work was supported by the European Research Council under G.A. ERC-StG 638284, by EU H2020 Program under G.A. 874827 (BRAV3), by Ministerio de Ciencia e Innovación (Spain) through project PID2019-105674RB-I00 and by European Social Fund (EU) and Aragón Government through BSICoS group (T39_20R).

References

[1] Leor J, Amsalem Y, Cohen S. Cells, Scaffolds, and Molecules for Myocardial Tissue Engineering. Pharmacology Therapeutics February 2005;105(2):151–163. ISSN 01637258.

[2] Gao L, Kupfer ME, Jung JP, Yang L, Zhang P, Da Sie Y, Tran Q, Ajeti V, Freeman BT, Fast VG, Campagnola PJ, Ogle BM, Zhang J. Myocardial Tissue Engineering With Cells Derived From Human-Induced Pluripotent Stem Cells and a Native-Like, High-Resolution, 3-Dimensionally Printed Scaffold. Circulation Research April 2017;120(8):1318–1325. ISSN 0009-7330, 1524-4571.

[3] Khan M, Xu Y, Hua S, Johnson J, Belevych A, Janssen PML, Gyorke S, Guan J, Angelos MG. Evaluation of Changes in Morphology and Function of Human Induced Pluripotent Stem Cell Derived Cardiomyocytes (HiPSC-CMs) Cultured on an Aligned-Nanofiber Cardiac Patch. PLOS ONE May 2015;10(5):e0126338. ISSN 1932-6203. Publisher: Public Library of Science.

[4] Castilho M, Mil Av, Maher M, Metz CHG, Hochleitner G, Groll J, Doevendans PA, Ito K, Sluijter JPG, Malda J. Melt Electrowriting Allows Tailored Microstructural and Mechanical Design of Scaffolds to Advance Functional Human Myocardial Tissue Formation. Advanced Functional Materials 2018;28(40):1803151. ISSN 1616-3028.

[5] Cantwell C, Roney C, Ng F, Siggers J, Sherwin S, Peters N. Techniques for Automated Local Activation Time Annotation and Conduction Velocity Estimation in Cardiac Mapping. Computers in Biology and Medicine October 2015; 65:229–242. ISSN 0010-4825.

[6] Durrer D, Van Dam RT, Freud GE, Janse MJ, Meijler FL, Arzbaecher RC. Total Excitation of the Isolated Human Heart. Circulation June 1970;41(6):899–912. ISSN 0009-7322, 1524-4539.

[7] Paci M, Koivumäki JT, Lu HR, Gallacher DJ, Passini E, Rodriguez B. Comparison of the Simulated Response of Three in Silico Human Stem Cell-Derived Cardiomyocytes Models and in Vitro Data Under 15 Drug Actions. Frontiers in Pharmacology 2021;12. ISSN 1663-9812. Publisher: Frontiers.

[8] Jung A, Staat M. Modeling and Simulation of Human Induced Pluripotent Stem Cell-Derived Cardiac Tissue. GAMM Mitteilungen 2019;42(4):e201900002. ISSN 1522-2608.

[9] Paci M, Hyttinen J, Aalto-Setälä K, Severi S. Computational Models of Ventricular- and Atrial-Like Human Induced Pluripotent Stem Cell Derived Cardiomyocytes. Annals of Biomedical Engineering November 2013; 41(11):2334–2348. ISSN 0090-6964, 1573-9686.

[10] Mountris KA, Pueyo E. Next-Generation in Silico Cardiac Electrophysiology Through Immersed Grid Meshfree Modeling: Application to Simulation of Myocardial Infarction. In 2020 Computing in Cardiology. IEEE, 2020; 1–4.

[11] Mountris KA, Pueyo E. The Radial Point Interpolation Mixed Collocation (RPIMC) Method for the Solution of the Reaction-Diffusion Equation in Cardiac Electrophysiology. In International Conference on Computational & Experimental Engineering and Sciences. Springer, 2021; 39–44.

[12] Mountris KA, Pueyo E. A Dual Adaptive Explicit Time Integration Algorithm for Efficiently Solving the Cardiac Monodomain Equation. International Journal for Numerical Methods in Biomedical Engineering 2021;37(7):e3461.

[13] Spach MS, Miller WT, Geselowitz DB, Barr RC, Kootsey JM, Johnson EA. The Discontinuous Nature of Propagation in Normal Canine Cardiac Muscle. Evidence for Recurrent Discontinuities of Intracellular Resistance that Affect the Membrane Currents. Circulation Research January 1981; 48(1):39–54. ISSN 0009-7330, 1524-4571.

[14] Pérez-Zabalza M, Diez E, Rhyins J, Mountris KA, Vallejo-Gil JM, Fresneda-Roldán PC, Fañanás-Mastral J, Matamala-Adell M, Sorribas-Berjón F, Vázquez-Sancho M, Ballester-Cuenca C, Segovia-Roldán M, Oliván-Viguera A, Pueyo E. Improved Methods for Processing Optical Mapping Signals From Human Left Ventricular Tissues at Baseline and Following Adrenergic Stimulation. 2020 Computing in Cardiology 2020;1–4.

Address for correspondence:

Ricardo M. Rosales

University of Zaragoza, Campus Río Ebro, I+D Building, D-5.01.1B, Mariano Esquillor, s/n street, 50018, Zaragoza, Spain

rrosales@unizar.es